Inorganica Chimica Acta 365 (2011) 282–289

Contents lists available at ScienceDirect

Inorganica Chimica Acta

journal homepage: www.elsevier.com/locate/ica

Synthesis and structural characterization of two new copper(II) complexes with thiazoline derivative ligands: Influence of the coordination on the phagocytic activity of human neutrophils

A.M. Lozano-Vila [a], F. Luna-Giles [a,*], E. Viñuelas-Zahínos [a], F.L. Cumbrera [b], A.L. Ortiz [c], F.J. Barros-García [a], A.B. Rodríguez [d]

[a] Departamento de Química Orgánica e Inorgánica, Facultad de Ciencias, Universidad de Extremadura, 06071 Badajoz, Spain
[b] Departamento de Física, Facultad de Ciencias, Universidad de Extremadura, 06071 Badajoz, Spain
[c] Departamento de Ingeniería Mecánica, Energética y de los Materiales, Escuela de Ingenierías Industriales, Universidad de Extremadura, 06071 Badajoz, Spain
[d] Departamento de Fisiología, Facultad de Ciencias, Universidad de Extremadura, 06071 Badajoz, Spain

ARTICLE INFO

Article history:
Received 20 May 2010
Received in revised form 15 September 2010
Accepted 20 September 2010
Available online 29 September 2010

Keywords:
Tetrahydrothiazine
Thiazoline
Thiazolidine
Copper(II) complexes
Human neutrophils
Phagocytosis

ABSTRACT

Two new copper(II) complexes dichloro[2-(3,4-dichlorophenyl)imine-κ*N*-(2-thiazolin-κ*N*-2-yl)thiazolidine]copper(II) [$CuCl_2$(TdTn)] (**1**) and dichloro[2-(3,4-dichlorophenyl)imine-κ*N*-(2-thiazolin-κ*N*-2-yl)tetrahydrothiazine]copper(II) [$CuCl_2$(TzTn)] (**2**) were synthesized, then characterized by elemental analysis, UV–Vis–NIR diffuse reflectance, electron paramagnetic resonance (EPR) spectroscopy, magnetic susceptibility, infrared spectroscopy, and finally their crystal structures determined by X-ray diffractometry. The structural determination of [$CuCl_2$(TzTn)] (**2**) was made by conventional single-crystal diffractometry, whereas the procedure followed to resolve the crystal structure of [$CuCl_2$(TdTn)] (**1**) by means powder diffractometry using direct-space methods with a 'Monte–Carlo/parallel tempering' search algorithm. A final refinement of the crystal structure was performed using the Rietveld method. It was found that the environment around the copper(II) ion for both complexes can be described as having a distorted tetrahedral geometry, with the metallic atom coordinated with two chlorides, one imine nitrogen and one thiazoline nitrogen. The biological activity of the complexes, inorganic salt and their ligands has been evaluated by examining their phagocytic activity on human neutrophils. This activity enhances in the case of the samples treated with [$CuCl_2$(TdTn)] (**1**) and [$CuCl_2$(TzTn)] (**2**) with respect to the ones to which $CuCl_2$, TdTn or TzTn was added.

1. Introduction

Phagocytosis is one of the principal processes by which the innate immune system eliminates invading microorganisms or foreign materials. One type of phagocytes is the neutrophils which are able to recognize pathogens, migrate to the site of invasion, engulf the particles or microorganisms, and kill or degrade them by means of a specialized mechanism termed the respiratory burst. This mechanism is characterized by the generation of reactive oxygen intermediates such as superoxide anion, hydroxyl radical, hydrogen peroxide, and singlet oxygen. These reactive oxygen species, which are responsible for killing phagocytosed organisms, are controlled by various enzymes, including NADPH-oxidase, superoxide dismutase, peroxidase, and catalase [1,2].

Copper plays an important role in the development and maintenance of the immune system, and its deficiency increases susceptibility to such infections as Menkes's disease which causes infections in the respiratory tract of infants [3]. Copper deficiency reduces both the number of neutrophils in human peripheral blood and their ability to generate superoxide anion and kill ingested microorganisms [4]. While the immunity dysfunction produced by copper deficiency is resolved by copper supplementation, an excess of copper may have adverse effects on the immune system, including phagocytic activity [5].

A few years ago, a copper complex, [$Cu(KTZ)_3Cl_2$], in which the KTZ ligand is the antimycotic ketoconazole [6], was reported to enhance the phagocytic capacity activity of human neutrophils. However, the crystal structure of this copper complex was not investigated by X-ray diffractometry [7], probably because it could not be crystallized with the required size and quality for conventional single-crystal diffractometry. Indeed, this is unfortunately the case for many substances of chemical and biological interest. In these situations, the crystal structure can be determined by the alternative method of X-ray powder diffractometry (XRPD).

In the present work, we report the novel synthesis and characterization of two new copper(II) complexes, one with the organic ligand [2-(3,4-dichlorophenyl)imine-*N*-(2-thiazolin-2-yl)thiazolidine]

* Corresponding author. Tel./fax: +34 924289397.
E-mail address: pacoluna@unex.es (F. Luna-Giles).

0020-1693/$ - see front matter © 2010 Elsevier B.V. All rights reserved.
doi:10.1016/j.ica.2010.09.031

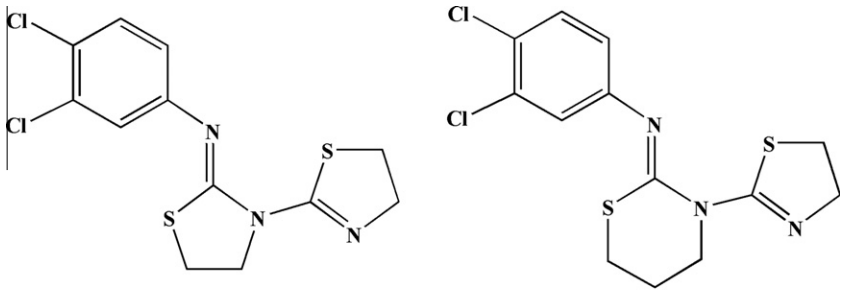

Scheme 1.

(TdTn) and a second one with [2-(3,4-dichlorophenyl)imine-*N*-(2-thiazolin-2-yl)tetrahydrothiazine (TzTn), whose structures contain thiazoline, thiazolidine, and 1,3-thiazine rings (see Scheme 1). These heterocycles form part of natural biologically-active products with antibiotic properties, examples being micacocidin [8,9], the penicillins [10], and the cephalosporins [11]. In addition to this structural study, we also investigated the influence of the coordination on the phagocytic activity of human neutrophils, motivated by the fact that the coordination of zinc(II) with TdTn has been shown to improve the phagocytosis stimulating effect of TdTn [12], an example of the biological activity of a compound being enhanced by coordination or chelation with metal ions.

2. Experimental

2.1. General procedures

All reagents were commercial grade material and were used without further purification. The ligands [2-(3,4-dichlorophenyl) imino-*N*-(2-thiazolin-2-yl)thiazolidine] (TdTn) and [2-(3,4-dichlorophenyl)imino-*N*-(2-thiazolin-2-yl)tetrahydrothiazine (TzTn) were synthesized according to reported procedures [13] and [14], respectively.

Chemical analyses of carbon, hydrogen, nitrogen, and sulphur were performed by microanalytical methods using a Leco CHNS-932 microanalyser. IR spectra were recorded on a Perkin–Elmer FT-IR 1720 spectrophotometer, from KBr pellets in the 4000–370 cm^{-1} range and on a Perkin–Elmer FT-IR 1700X spectrophotometer, from polyethylene pellets in the 500–150 cm^{-1} range. Solid state electronic spectra for complexes in the 200–1500 nm range were obtained from pellets of the samples, using a Shimadzu UV-3101 PC spectrophotometer and $BaSO_4$ as a reference. Magnetic susceptibility measurements were performed on polycrystalline samples using a magnetometer with pendulum MANICS DSM8, equipped with helium continuous-flow cryostat and an electromagnetometer DRUSCH EAF 16 UE. Data were corrected for temperature independent paramagnetism and diamagnetic contributions, which were estimated from the Pascal constants. EPR spectra were recorded at room temperature in solid state and at 77 K in frozen DMSO employing a BRUKER ESP-300E spectrometer using the X band of microwave.

2.2. Preparation of [$CuCl_2$(TdTn)] (**1**)

This complex was isolated from a freshly prepared ethanolic (96%) solution (1 mL) of $CuCl_2{\cdot}2H_2O$ (51.3 mg, 0.30 mmol) that was added to an ethanol solution (15 mL) of TdTn (100 mg, 0.30 mmol). The resulting solution was allowed to evaporate slowly at room temperature. After a few days, green crystals were isolated from the solution (82 mg, 58.4%). The crystals were separated by filtration, washed with cold ether and air-dried. *Anal*. Calc. for $C_{12}H_{11}Cl_4CuN_3S_2$: C, 30.88; H, 2.38; N, 9.00; S, 13.74. Found: C, 30.98; H, 2.65; N, 8.70; S, 14.02%. IR (KBr): *ν*(C=N) 1614, (thiazoline ring vibrations) 1538, 1000, 953, 773, 724, 633, 589, 534, 444 (thiazolidine ring vibrations) 1032, 916, 827, 700, 673, 484, 408 cm^{-1}.

2.3. Preparation of [$CuCl_2$(TzTn)] (**2**)

The [$CuCl_2$(TzTn)] complex was isolated from an ethanolic (96%) solution (1 mL) of $CuCl_2{\cdot}2H_2O$ (49.2 mg, 0.29 mmol) that was added to an ethanol–water solution (15 mL) of TzTn (100 mg, 0.29 mmol). The resulting solution was allowed to evaporate slowly at room temperature. After a few days, green crystals were isolated from the solution (94 mg, 67.7%). The crystals were first separated by filtration, then washed with cold ether and finally air-dried. *Anal*. Calc. for $C_{13}H_{13}Cl_4CuN_3S_2$: C, 32.50; H, 2.73; N, 8.74; S, 13.30. Found: C, 32.35; H, 2.78; N, 8.85; S, 12.98%. IR (KBr): *ν*(C=N) 1594 (thiazoline ring vibrations) 1524, 962, 947, 778, 757, 721, 647, 604, 551, 455, 444 (tetrahydro-1,3-thiazine ring vibrations) 1027, 911, 836, 828, 695, 674, 659, 587, 400 cm^{-1}.

2.4. Isolation of neutrophils

Neutrophils were isolated by adding in thin glass tubes and in the following order, 2.5 mL of 1119 Histopaque (Sigma–Aldrich) separating medium, 2.5 mL of 1077 Histopaque (Sigma–Aldrich) separating medium and 2.5 mL of human peripheral blood from six healthy volunteers who were not treated with antibiotics, anti-inflammatories or anticoagulants, in order to not affect cell adherence (this was not necessary for cell viability). The samples were then centrifuged at 600*g* for 15 min at room temperature. The halo of neutrophils was withdrawn using a glass Pasteur pipette and washed with PBS medium in plastic tubes. The supernatant was discarded and the tube was beaten so that cells detached. Then, 2 mL of Hank's medium was added and the pellet resuspended. Cells were counted in a Neubauer haemocytometer under phase contrast microscopy at 40×, and the suspension was adjusted to 5×10^5 neutrophils/mL.

2.5. Cell viability

To study the cell viability and the phagocytosis of latex beads the tested substances were dissolved in H_2O:DMSO (9:1). Cell viability was assessed using calcein as fluorescent probe. For calcein loading, cells were incubated for 45 min with 1 M calcein AM at 37 °C and centrifuged 10 min at 480*g*, resuspending the pellet in fresh Na-HEPES buffer. Aliquots of 2 mL of the cell suspension were treated with 1×10^{-3} mM $CuCl_2$, TdTn, TzTn, complexes **1** and **2** for 30 min at room temperature, then cells were centrifuged and

resuspended in fresh buffer. Finally, the calcein fluorescence remaining in the cells after treatments with these substances was recorded using a Shimadzu RF-5301-PC fluorescence spectrophotometer. Samples were excited at 490 nm and the resulting fluorescence was measured at 510 nm.

2.6. Phagocytosis of latex beads

Aliquots of 200 μL of Hank's cellular suspension were put into the wells of plastic macrophage migration inhibition factor (MIF)-type plaques (AFORA, Spain), following the method described by Rodríguez et al. [15]. After 30 min incubation at 37 °C in a stove, the adhered monolayer was washed with PBS at 37 °C. Then, 200 μL of Hank's medium, 20 μL of latex beads (1.1×10^{-3} mm, diluted to 1% in DMSO; Sigma) and 3 μL of ligand or complex 1×10^{-4} M, yielding a final concentration of 1.3×10^{-3} mM (3 μL of H_2O:DMSO (9:1) for control) were added, following by another 30 min incubation at 37 °C in a stove. Finally, the samples were washed with PBS, fixed with methanol 5 min and stained with eosin (five passes) and haematoxylin (five passes). The plaques were carefully rinsed with tap water and dried, followed by counting under oil-immersion phase-contrast microscopy at 100×.

The number of particles ingested per 100 neutrophils was expressed as the latex-bead phagocytosis index (P.I.). The percentage of cells that had phagocytosed at least one latex bead was expressed as the phagocytosis percentage (P.P.). The ratio P.I./P.P. was calculated, giving the phagocytosis efficiency (P.E.).

2.7. Statistical analysis

The results of the biological study were analyzed using the ANOVA-Scheffe's *F*-test. $P < 0.05$ was considered statistically significant. Data were expressed as the mean (X) ± standard error (SE) of six experiments, performed in duplicate. In the phagocytosis studies, results were referred to 100% of the control to avoid the dispersion due to the great variability of patients' cells phagocytic activity.

2.8. Crystal structure determinations

Crystals of the TzTn ligand and complex **2** with the appropriate size and quality for X-ray single-crystal diffractometry were isolated and used for the structural analysis. Unfortunately, this was not possible for complex **1** and therefore their crystal structure was determined by X-ray powder diffractometry.

The experimental details of the crystal structure determination, including crystal data, data collection, structure determination, and refinement are listed in Table 1 for the ligand and complex **2**. X-ray single-crystal diffraction measurements were performed using a Bruker SMART CCD diffractometer with Mo Kα radiation (λ = 0.71073 Å, graphite monochromator). The first fifty frames were measured at the end of data collection to monitor instrument and crystal stability. The data were empirically corrected for absorption and other effects using the SADABS [16] program. The structures were solved by direct methods and subsequent Fourier differences using the SHELXS-97 [17] program and refined by full-matrix least-squares on F^2 with SHELXL-97 [18], included in WINGX [19] package assuming anisotropic displacement parameters for non-hydrogen atoms, except for C(3A), C(2B) and C(6B) disordered atoms with isotropic displacement parameters. In the structure of TzTn, the thiazoline ring of both independent molecules and the thiazine ring of second one show a disorder affecting C(3A), C(2B) and C(6B) atoms, being the value of the refined occupancy 0.57(1) for C(3A) and 0.43(1) for C(3A2) in first independent molecule and 0.48(2) for C(2B), 0.52(2) for C(2B2), 0.59(1) for C(6B) and 0.41(1) for C(6B2) in second one. All hydrogen atoms attached to carbon and nitrogen atoms were positioned geometrically, with U_{iso} values derived from U_{eq} values of the corresponding carbon and nitrogen atoms. Diagrams were generated using ORTEP3 for Windows [20]. A summary of the crystal data, experimental details and refinement results are listed in Table 1.

Table 1
Crystal data, data collection and refinement details for TzTn and **2**.

	TzTn	**2**
Crystal shape	prism	prism
Colour	colourless	green
Size (mm)	0.58 × 0.38 × 0.35	0.42 × 0.36 × 0.32
Chemical formula	$C_{13}H_{13}Cl_2N_3S_2$	$C_{13}H_{13}Cl_4CuN_3S_2$
Formula weight	346.28	480.72
Crystal system	triclinic	monoclinic
Space group	$P\bar{1}$	$P2_1/c$
Unit cell dimensions		
a (Å)	10.967(1)	9.873(1)
b (Å)	12.163(1)	17.386(1)
c (Å)	12.829(1)	10.386(1)
α (°)	85.505(1)	
β (°)	80.517(1)	96.361(1)
γ (°)	64.147(1)	
Cell volume (Å^3)	1519.0(2)	1771.8(2)
Z	4	4
D_{calc} (g cm^{-3})	1.5514	1.802
μ (mm^{-1})	0.694	2.071
F(0 0 0)	712	964
2θ range	3.2–56.7	4.2–58.3
Index ranges	$-14 \leqslant h \leqslant 14$, $-15 \leqslant k \leqslant 15$ $-16 \leqslant l \leqslant 16$	$-13 \leqslant h \leqslant 13$, $-22 \leqslant k \leqslant 22$, $-14 \leqslant l \leqslant 14$
Independent reflections	6880	3923
Observed reflections	5706[$F > 4.0\sigma(F)$]	3552[$F > 4.0\ \sigma(F)$]
Maximum/minimum transmission	0.7832/0.7289	0.5571/0.4767
Number of refined parameters	358	208
R [$I > 2\sigma(I)$][a]	0.049	0.030
wR [$I > 2\sigma(I)$][b]	0.125	0.077
GOF[c]	1.034	1.102
$\rho_{maximum}$, $\rho_{minimum}$ (e Å^{-3})	0.652, −0.583	0.756, −0.472

[a] $R = \Sigma||F_o| - |F_c||/\Sigma|F_o|$.

[b] $R = \left\{\Sigma\left[w\left(F_o^2 - F_c^2\right)^2\right]/\Sigma\left[w\left(F_o^2\right)^2\right]\right\}^{1/2}$.

[c] The goodness-of-fit (GOF) equals $\left\{\Sigma\left[w\left(F_o^2 - F_c^2\right)^2\right]/(N_{rf\,ln\,s} - N_{params})\right\}^{1/2}$.

The XRD pattern for the structural determination of complex **1** was obtained via conventional powder diffractometry. Before data collection, the powder particles resulting from the synthesis of complex **1** were ground ultra-fine to avoid texture and graininess effects in the XRPD pattern. The resulting powder was then loaded into the holder (3-mm thick), and pressed slightly with a glass slide to ensure a flat surface and thus the absence of instrumental shift in the position of the XRPD peaks. Table 2 gives the specific experimental and set-up conditions used. The determination of the crystal structure of complex **1** was performed from its XRPD pattern by successive stages of molecular modeling, direct-space methods, and Rietveld refinement. Firstly, the most stable conformation of the isolated molecule was obtained by molecular modeling with a semi-empirical quantum-chemical model using the HYPERCHEM program [21]. Subsequently, a first estimate of the crystal structure was obtained by means of direct-space methods with Monte Carlo algorithms and the "parallel tempering" formulation using the FOX program [22]. This was done using as input the orthorhombic unit cell and space group (Pbcn) determined by indexing and analyzing the first 30 XRD peaks with the CRYSFIRE and CHECKCELL programs [23,24]. Lastly, the so-determined crystal structure was refined

Table 2
Details of the data collection, structure solution and refinement for **1**.

Colour	Green
Chemical formula	$C_{12}H_{11}Cl_4CuN_3S_2$
Crystal system	orthorhombic
Space group	Pbcn
Unit cell dimensions	
a (Å)	17.88840(14)
b (Å)	8.91130(8)
c (Å)	23.59260(23)
Cell volume (Å^3)	3760.87(5)
Z	8
2θ range	5–100
Step scan increment (°), counting time (s)	0.02, 20
Number of reflections	2046
Number of atoms (H excluded)	22
Number of global parameters refined	117
Number of profile parameters refined	10
Number of structural parameters refined	55
R_{wp}, R_p, χ^2_r	0.091, 0.064, 8.51

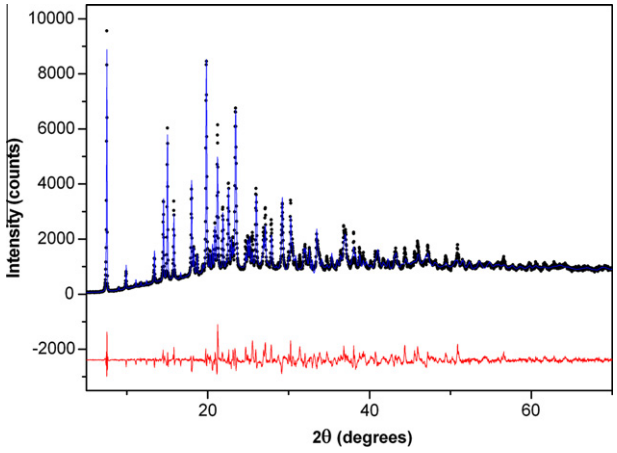

Fig. 1. Plot output from the Rietveld analysis of the X-ray diffraction pattern corresponding to **1**. Points are the experimental X-ray diffraction data; the solid line is the calculated pattern; the residuals are plotted at the bottom.

by the Rietveld method using the FULLPROF program [25]. The Rietveld refinement, which was made by first taking the molecules to be rigid bodies and then replacing the rigid-body constraints by soft restraints on the atom–atom angles and distances, included the typical crystallographic, profile, and instrumental aspects [14,26–28]. The residuals at the completion of the Rietveld refinement were $R_{wp} = 0.091$ and $R_p = 0.064$, and the refined cell parameters were $a = 17.88840(14)$ Å, $b = 8.91130(8)$ Å, and $c = 23.59260(23)$ Å. Fig. 1 shows the Rietveld refinement plot output and Table 2 lists the most representative crystallographic parameters of this structure.

3. Results and discussion

3.1. Description of the crystal structures

The single crystal X-ray diffraction analysis has revealed that TzTn crystallizes in the triclinic system with two independent molecules in the asymmetric unit cell. The overall view and labeling of the atoms in two independent molecules are displayed in Fig. 2. Table 3 lists the selected bond lengths and angles.

In the S(1)–C(1)–N(1)–C(2)–C(3) rings, the short endocyclic C=N bonds [C(1A)–N(1A) = 1.267(3) Å; C(1B)-N(1B) = 1.265(3) Å] are accompanied by high N–C–S angles [N(1A)–C(1A)–S(1A) = 118.0(2)°; N(1B)–C(1B)–S(1B) = 118.1(2)°] and relatively long S^{II}–C(sp^2) bonds [S(1A)–C(1A) = 1.767(2) Å; S(1B)–C(1B) = 1.773(3) Å], which are characteristic of a thiazoline ring [29]. In contrast, in the S(2)–C(4)–N(2)–C(5)–C(6)–C(7) rings, the endocyclic C–N bonds [C(4A)–N(2A) = 1.387(3) Å; C(4B)–N(2B) = 1.383(3) Å] are longer to the exocyclic C=N bonds [C(4A)–N(3A) = 1.266(3) Å; C(4B)–N(3B) = 1.266(3) Å], the S–C(sp^2) bonds [S(2A)–C(4A) = 1.763(2) Å; S(2B)-C(4B) = 1.763(2) Å] and the S-C-N angles [S(2A)–C(4A)–N(2A) = 121,4(2)°; S(2B)–C(4B)–N(2B) = 121,1(2)°]; are lower to those found in a 1,3-thiazine ring [12] which we seems indicate an imine-tetrahydro-1,3-thiazine form.

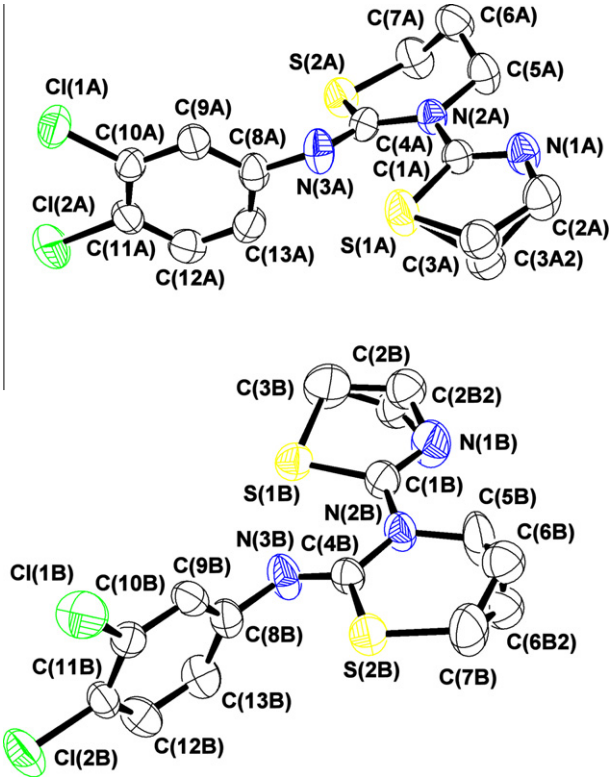

Fig. 2. The atom numbering scheme for two molecules on TzTn constituting the asymmetric unit of the structure. The thermal ellipsoids are plotted at the 50% probability level.

It is known that the imine tautomers can exist as two geometrical isomers, *syn* (Z) and *anti* (E), but in both crystals of two ligands, only Z isomers have been observed.

We discuss next the crystal structure of copper complexes, although our interpretation of complex **1** should be treated with caution since the crystallographic data were determined from powder diffractometry.

The structure of copper complexes consists of discrete neutral monomeric units in which the environment around the copper(II) atom may be described as a distorted tetrahedral geometry. In both complexes, the metallic atom is coordinated by two chloride atoms, one imine nitrogen and one thiazoline nitrogen. A diagram of the molecular structures and the atom numbering system used is shown in Figs. 3 and 4. The most relevant bond lengths and angles are given in Table 4.

The Cu–Cl bond lengths [Cu–Cl(1) and Cu–Cl(2) in **1**; Cu–Cl(2) in **2**] are slightly shorter than the calculated average value [2.248(34) Å] for 291 tetrahedral copper(II) complexes with a Cl_2N_2 coordination environment around Cu(II) ion, obtained with CONQUEST software [30] from the Cambridge Structural Database (CSD, Version v5.31, Feb. 2010) [31]. However, the Cu–Cl(1) distance in **2** is slightly longer than the aforementioned mean value.

Table 3
Selected bond lengths (Å), angles (°) and hydrogen-bond parameters for TzTn.

S(1A)–C(1A)	1.767(2)	S(1B)–C(1B)	1.773(3)
S(2A)–C(4A)	1.763(2)	S(2B)–C(4B)	1.763(2)
N(1A)–C(1A)	1.267(3)	N(1B)–C(1B)	1.265(3)
N(2A)–C(1A)	1.399(3)	N(2B)–C(1B)	1.397(3)
N(2A)–C(4A)	1.387(3)	N(2B)–C(4B)	1.383(3)
N(3A)–C(4A)	1.266(3)	N(3B)–C(4B)	1.266(3)
N(3A)–C(8A)	1.412(3)	N(3B)–C(8B)	1.406(3)
C(1A)–N(1A)–C(2A)	119.9(2)	C(1B)–N(1B)–C(2B)	106.3(4)
C(1A)–N(2A)–C(4A)	121.0(2)	C(1B)–N(2B)–C(4B)	121.6(2)
N(1A)–C(1A)–S(1A)	118.0(2)	N(1B)–C(1B)–S(1B)	118.1(2)
N(1A)–C(1A)–N(2A)	119.8(2)	N(1B)–C(1B)–N(2B)	119.6(2)
N(2A)–C(1A)–S(1A)	122.2(2)	N(2B)–C(1B)–S(1B)	122.3(2)
N(2A)–C(4A)–S(2A)	121.3(2)	N(2B)–C(4B)–S(2B)	121.0(3)
N(3A)–C(4A)–N(2A)	119.4(2)	N(3B)–C(4B)–N(2B)	120.1(2)
C(4A)–N(3A)–C(8A)	122.2(2)	C(4B)–N(3B)–C(8B)	122.6(2)

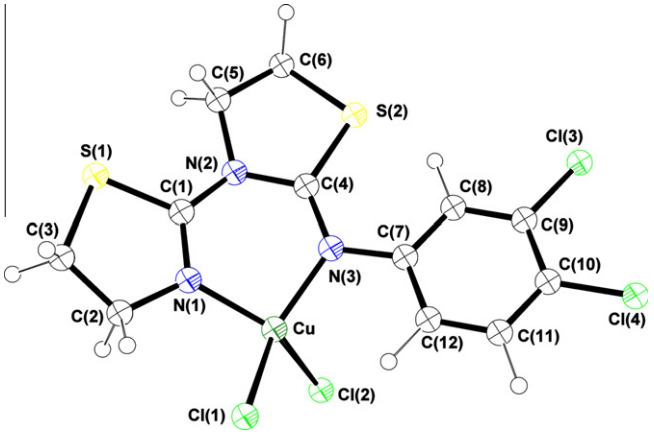

Fig. 3. Molecular structure of **1** showing the atom-numbering scheme. The thermal ellipsoids are drawn at a 50% level.

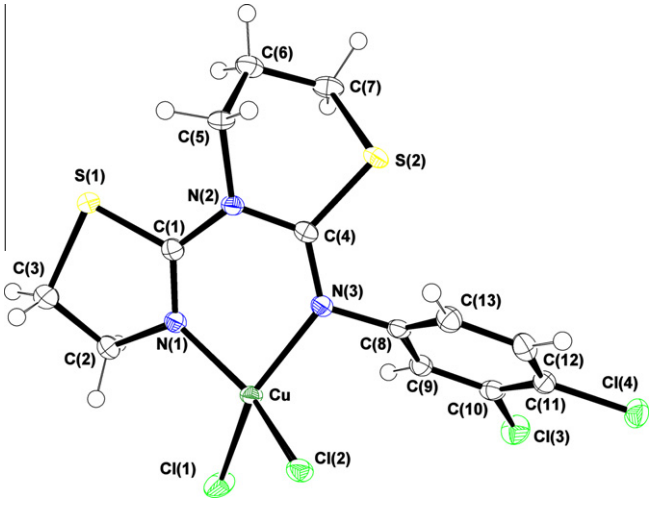

Fig. 4. Molecular structure of **2** showing the atom-numbering scheme. The thermal ellipsoids are drawn at a 50% level.

Likewise, the Cu–N_{imine} bond distances are similar than the mean value [1.965(63) Å] calculated for 121 tetrahedral copper(II) complexes in CSD [31]. The Cu–$N_{thiazoline}$ bond distances are slightly shorter than the corresponding mean value [1.963(39) Å] found for 18 copper(II) complexes with Cu–$N_{thiazoline}$ bonds in CSD [31]. The distortion of the tetrahedral environment of the copper(II) ion

Table 4
Selected bond lengths (Å) and angles (°) for **1** and **2**.

	1	**2**
Cu–Cl(1)	2.180(5)	2.316(1)
Cu–Cl(2)	2.188(2)	2.197(1)
Cu–N(1)	1.914(8)	1.949(2)
Cu–N(3)	1.932(16)	2.046(2)
Cl(1)–Cu–Cl(2)	97.2(2)	98.3(1)
N(3)–Cu–Cl(1)	143.1(9)	145.6(1)
Cl(2)–Cu–N(3)	99.1(6)	95.3(1)
N(1)–Cu–Cl(1)	94.8(3)	99.6(1)
Cl(2)–Cu–N(1)	137.0(4)	144.7(1)
N(3)–Cu-N(1)	95.5(11)	86.8(1)

in **2** is larger than in **1**, being indicated by the ligand–metal–ligand bite angles [that vary between 143.1(9)° and 94.8(3)° in **1** and 145.6(1)° and 86.8(1)° in **2**] and by the dihedral angle between the planes Cl(1)–Cu–Cl(2) y N(1)–Cu–N(3) are [54.6° in **1** and 48.3° in **2**].

As it can be seen in Figs. 3 and 4, thiazoline rings rotate around C(1)–N(2) bond in such a way that the N(1) and N(3) atoms are on the same side in order to coordinate to copper(II) ion. This is demonstrated by the values of the correspondent torsion angles: S(1)–C(1)–N(2)–C(5) = 7.3(1)° in **1**, −175.6(2)° in TdTn [12]; S(1)–C(1)–N(2)–C(5) = 6.5° in **2**; 177.9° and −178.2° in unit A and B of TzTn, respectively.

At last, there has been an increase of the distance N(3)–C(7) (in **1**) and N(3)–C(8) (in **2**) with respect to the respective ligand: N(3)–C(7) = 1.421(2) Å in TdTn [12], 1.455(1) Å in **1**; N(3)–C(8) = 1.413(4) Å and 1.403(4) Å in unit A and B of TzTn, respectively, 1.418(3) Å in **2**. This could be due to the lost of electronic density of the imine nitrogen atom when coordinates the metallic ion.

3.2. Electronic spectra

The electronic reflectance spectra of the copper(II) complexes are very close which is a consequence of molecular structure similarity. They were consisted of two strong bands at 35710 and 24940 cm^{-1} for complex **1** and at 32360 and 24270 cm^{-1} for complex **2**. For both compounds the bands registered around 34000 cm^{-1} are assigned to the ligand's $\pi \rightarrow \pi^*$ transition [14,32] whereas the bands registered near to 24000 cm^{-1} are assigned to the chlorine-to-copper change transfer transition [33]. There were also two d–d bands of equal intensity at 10640 and 14770 cm^{-1} for **1** and at 10170 and 14430 cm^{-1} for **2**, which are consistent with a compressed tetrahedral geometry [34,35] in accord with the dihedral angle values between N–Cu–N and Cl–Cu–Cl obtained means X-ray diffraction data.

For a distorted tetrahedral symmetry flattening towards *xy* plane, the energetic d orbitals sequence would be $d_{xy} > d_{xz}$, $d_{yz} > d_{x2-y2} > d_{z2}$ [36]. However, in complexes with bidentate ligands the distortion is not uniaxial and all the degeneracy is removed. For these copper(II) complexes with a $CuCl_2N_2$ chromophore group and C_{2v} symmetry (if only the atoms bonded to the metal are considered) $^2E(D)$ state splits to $^2A_1$ and $^2A_2$ terms whereas $^2T_2(D)$ state splits to A_1, B_1 and B_2 and the energetic d orbital sequence is $d_{x2-y2} > d_{xy} > d_{xz} > d_{z2} > d_{yz}$ [37,38]. Thus the bands centered at 10 640 cm^{-1} for **1** and 10 170 cm^{-1} for **2** correspond to $^2A_2(E)[(d_{xy})^1] \leftarrow {}^2A_1(T_2)[(d_{x2-y2})^1]$ and $^2B_1(T_2)[(d_{xz})^1] \leftarrow {}^2A_1(T_2)[(d_{x2-y2})^1]$ transitions and the bands at 14 470 cm^{-1} for **1** and at 14 430 cm^{-1} for **2** correspond to $^2A_1(E)[(d_{z2})^1] \leftarrow {}^2A_1(T_2)[(d_{x2-y2})^1]$ and $^2B_2(T_2)[(d_{yz})^1] \leftarrow {}^2A_1(T_2)[(d_{x2-y2})^1]$ transitions.

Several authors have suggested a correlation between the spin allowed transitions caused by the ligand field splitting of a tetrahedral environment to square planar and the dihedral angle

Table 5
EPR parameters and far IR bands of copper complexes.

Compound	EPR parameters							Far IR bands (cm^{-1})		
	Solid (298 K)			DMSO (77 K)						
	g_{iso}	g||	$g\perp$	g||	$g\perp$	A||[a]	G	ν(Cu–$Cl_{terminal}$)	ν(Cu–N_{imine})	ν(Cu–$N_{thiazoline}$)
1	2.080			2.295	2.065	134	4.54	320 301	350	286
2		2.266	2.055	2.294	2.065	135	4.52	337 314	337	281

[a] Units: $\times 10^{-4}\,cm^{-1}$.

subtended by the ligands bonded at copper [39–41]. As the spectra of our compounds presents only two bands, we can to deduce that the difference of position between them increase with the dihedral angle. The higher separation between d–d transitions of complex **2** suggests a higher distortion degree of tetrahedral geometry, which is in good accord with the X-ray structural determination data.

3.3. Magnetic susceptibility measurements

The observed molar magnetic susceptibility for complexes **1** and **2** was corrected for diamagnetism and temperature-independent paramagnetism to provide the fully corrected magnetic moments at room temperature of 2.19 and 2.02 BM, respectively. These values can be considered in the range 1.75–2.20 BM typical for mononuclear copper(II) complexes without Cu–Cu interactions, regardless of the stereochemistry and independently of temperature, except at extremely low temperatures (<5 K) [42].

3.4. EPR data

The EPR spectra of **1** and **2** were recorded in the X-band using the 100 kHz field modulation for polycrystalline samples at 298 K and for samples in DMSO solution at 77 K.

The EPR parameters of copper(II) complexes are presented in Table 5.

The spectrum of **1** in the solid state at 298 K shows an isotropic profile ($g_{iso} = 2.08$). Such an isotropic spectrum gives no information on the electronic ground state of the copper(II) ion present in the compound. However, the spectrum of **2** at same temperature is typically axial with well-defined g|| and $g\perp$ values.

With respect to the EPR spectra of **1** and **2** in frozen DMSO at 77 K these show the presence of four hyperfine lines, which are characteristic of monomer copper(II) complexes [33] (no superhyperfine structure is observed). Likewise, the geometric parameter G [$G = (g|| - 2)/(g\perp - 2)$] in both complexes is found to be in the range 3.5–5.0, indicating a negligible exchange coupling among magnetically no equivalent copper(II) ions in the unit cell [43,44]. Moreover, the g values in the solid state at room temperature and in frozen solution for complex **2** are not much different from each other, hence the geometry around the copper ion is unaffected on cooling the solution to liquid nitrogen temperature.

The trend exhibited by the g values ($g|| > g\perp > 2.0023$) are consistent with a $(dx^2 - y^2)^1$ ground state of a compressed tetrahedral environment with a chromophore group $CuCl_2N_2$ [45,46].

3.5. IR spectra

The IR spectra of complexes **1** and **2** showed a strong $\nu(C{=}N)_{imine}$ absorption (at 1614 cm^{-1} in **1** and at 1594 cm^{-1} in **2**). These bands are shifted negatively relative to the uncoordinated imine function of the respective ligand [14,32]. Likewise, the in-plane stretching vibrations corresponding to $W_1[\nu(C{=}N)]$ skeletal vibration of the heterocyclic ring were also shifted to lower wavenumbers compared with that for the respective free ligand. From all this mentioned can be deduced a coordination via the imine nitrogens of the ligands [32,47–50].

In the low-frequency region, the C_1 symmetry of **1** and **2** cations predicts the appearance of four bands assignable to metal–ligand stretching vibrations. Tentative assignments are listed in Table 5. These bands have been assigned in good agreement with literature data. In this way, ν(Cu–Cl) vibrations are detected in copper(II) complexes with the chromophore group $CuCl_2N_2$ in the range 320–254 cm^{-1} [51]. Likewise, ν(Cu–N_{imine}) vibration is registered in several copper(II) complexes between 365 and 278 cm^{-1} [47–49,52,53], whereas ν(Cu–$N_{thiazoline}$) vibration are assigned between 253 and 222 cm^{-1} in complexes with this type of bonds [52–57].

3.6. Cell viability

The results obtained confirm that there is not any significant fall between the calcein fluorescence remaining in the cells before and after treatment, according to Scheffe F-test. This suggests that the treatment with $CuCl_2$, TdTn, TzTn, **1** and **2** does not cause any cellular damage under the work conditions and during the time our experiments lasted. The percentage of cells that were viable after the different treatments were: 99.6 ± 0.4 for $CuCl_2$, 84.0 ± 4.9 for TdTn, 84.7 ± 6.8 for TzTn, 83.4 ± 2.2 for **1**, 99.4 ± 0.5 for **2** and 87.5 ± 4.9 for the control sample H_2O:DMSO (9:1). Each value represents the mean ± standard error of six determinations performed in duplicate.

3.7. Study of the phagocytic function

The capacity of neutrophils to ingest latex beads, expressed as the phagocytosis index (Fig. 5A), increases as consequence of the treatment of neutrophils with our compounds, except with TzTn. This growth is statistically significant ($P < 0.05$) in the case of cells treated with **1** in comparison with control and the sample treated with TdTn. Likewise, for cells treated with **2** the growth is statistically significant ($P < 0.05$ or $P < 0.001$) in comparison with control, the sample treated with $CuCl_2$ and the sample treated with TzTn.

Likewise, the phagocytosis percentage (Fig. 5B) is significantly higher ($P < 0.05$) in the case of cells treated with **1** with respect to control and $CuCl_2$, which means that there are more active cells. Besides, this parameter is also significantly greater ($P < 0.001$) than control and TzTn in the case of the sample treated with TdTn. Finally, in the case of phagocytic efficiency for complexes **1** and **2** (Fig. 5C), this is higher in treated neutrophils. This percentage is significantly greater ($P < 0.05$ or $P < 0.001$) than the control values in the case of the samples treated with **1** (too with samples treated with $CuCl_2$ and TdTn) and with **2** (too with samples treated with $CuCl_2$, TzTn and **1**).

With respect to results obtained for similar zinc(II) complexes previously reported [12], cells treated with copper(II) complexes show a higher biological activity. Thus, cells treated with complex **2** have a significantly higher phagocytosis index and phagocytic

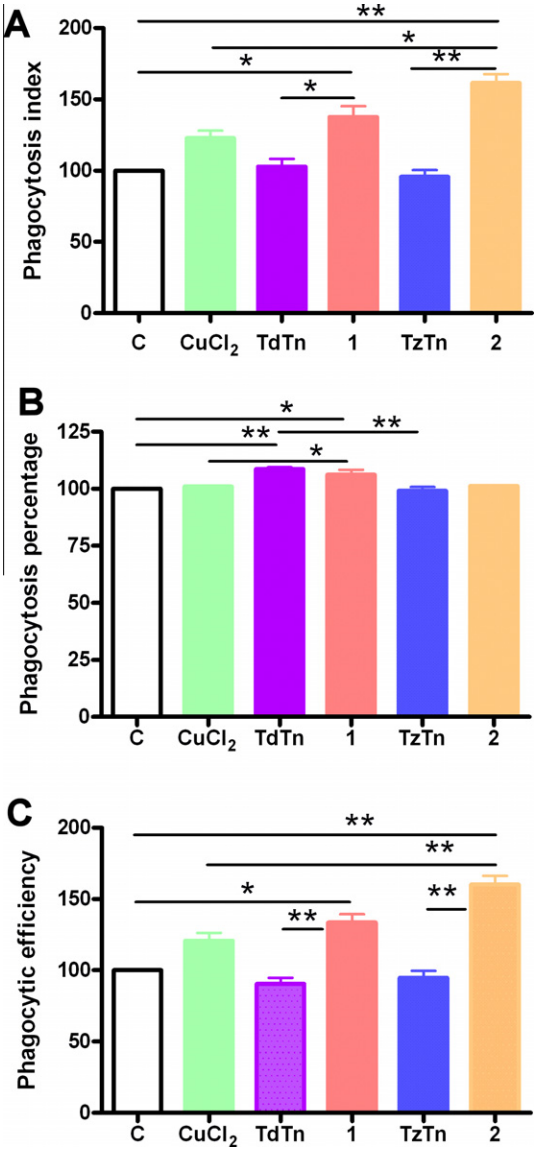

Fig. 5. Phagocytosis index (A), phagocytosis percentage (B) and phagocytic efficiency (C) variations of human neutrophils incubated in the presence of latex beads. Each value represents $X \pm SE$ of six determinations performed in duplicate. (*): $P < 0.05$; (**): $P < 0.001$.

efficiency than zinc(II) complexes. Likewise, cells treated with complex **1** show a significantly greater phagocytosis index than [$ZnCl_2$(TdTn)].

4. Conclusions

Ligands TdTn and TzTn act as bidentate ligands toward copper(II) ion through imine and thiazoline nitrogen atoms. The results of biological study indicate that the substances that more increase the phagocytic capacity of human neutrophils are complexes **1** and **2**. This phagocytosis promoting effect (reflected in the phagocytosis index) induced by **1** and **2** is due to both active phagocytes number increase (phagocytosis percentage) and a greater efficiency of these active cells phagocytizing antigenic particles (phagocytic efficiency). Besides, it is demonstrated that coordination to copper(II) improves neutrophils function, enhancing the non-specific immune response, since phagocytosis index and phagocytic efficiency are greater in the case of the samples treated with **2** and **1** with respect to the ones to which $CuCl_2$, TdTn or TzTn was added.

Acknowledgements

We would like to thank the Junta de Extremadura (III PRI+D+I) and the FEDER [Project PRI08A022] for financial support.

Appendix A. Supplementary material

CCDC 691948, 726711 and 726712 contain the supplementary crystallographic data for $CuCl_2$(TdTn), $CuCl_2$(TzTn) and TzTn, respectively. These data can be obtained free of charge from The Cambridge Crystallographic Data Centre via www.ccdc.cam.ac.uk/data_request/cif. Supplementary data associated with this article can be found, in the online version, at doi:10.1016/j.ica.2010.09.031.

References

[1] E. Bachere, E. Mialhe, J. Rodríguez, Fish Shellfish Immunol. 5 (1995) 597.
[2] M. Muñoz, R. Cedeño, J. Rodríguez, W.P.W. Van der Knapp, E. Mialhe, E. Bachère, Aquaculture 191 (2000) 89.
[3] P.C. Calder, Nutr. Clin. Métabol. 15 (2001) 286.
[4] S.S. Percival, Am. J. Clin. Nutr. 67 (1998) 1064.
[5] L.M. Gaetke, C.K. Chow, Toxicology 189 (2003) 147.
[6] M. Navarro, I. Colmenares, H. Correia, A. Hernández, Y. Ching, Y. Millán, L.E. Ojeda, M. Velásquez, G. Fraile, Arzneimittel-Forsch. 54 (2004) 746.
[7] M. Navarro, E.J. Cisneros-Fajardo, T. Lehmann, R.A. Sánchez-Delgado, R. Atencio, P. Silva, R. Lira, J.A. Urbina, Inorg. Chem. 40 (2001) 6879.
[8] A. Ino, A. Murabayashi, Tetrahedron 55 (1999) 10271.
[9] A. Ino, Y. Hasegawa, A. Murabayashi, Tetrahedron 55 (1999) 10283.
[10] J.D. Buynak, H. Chen, L. Vogeti, V.R. Gadhachanda, C.A. Buchanan, T. Alzkill, R.W. Shaw, J. Spencer, T.R. Walsh, Bioorg. Med. Chem. Lett. 14 (2004) 1299.
[11] G.C. Barrett, S.H. Eggers, T.R. Emersox, G. Löwe, J. Chem. Soc. (1964) 783.
[12] F.J. Barros-García, A. Bernalte-García, A.M. Lozano-Vila, F. Luna-Giles, J.A. Pariente, R. Pedrero-Marín, A.B. Rodríguez, J. Inorg. Biochem. 100 (2006) 1861.
[13] R.J. Outcalt, J. Heterocycl. Chem. 24 (1987) 1425.
[14] A.M. Lozano-Vila, F.L. Cumbrera, F. Luna-Giles, A.L. Ortiz, A. Bernalte-García, Z. Anorg. Allg. Chem. 633 (2007) 1801.
[15] A.B. Rodríguez, C. Barriga, M. de La Fuente, Agents Act. 31 (1990) 86.
[16] SADABS, Version 2.03, Bruker AXS Inc., Madison, WI, 2001.
[17] M. Sheldrick, SHELXS-97, Program for Crystal Structures Solution, University of Göttingen, Germany, 1997.
[18] M. Sheldrick, SHELXL-97, Program for Crystal Structures Refinement, University of Göttingen, Germany, 1997.
[19] L.J. Farrugia, J. Appl. Crystallogr. 32 (1999) 837.
[20] L.J. Farrugia, J. Appl. Crystallogr. 30 (1997) 565.
[21] HYPERCHEM. Release 5. Standalone Version. Computational Chemistry, Hypercube Inc., Publication HC50-00-03-00, October 1996, ISBN:1-896164-17-X.
[22] V. Favre-Nicolin, R. Cerný, FOX: A Program for ab initio Structure Solution From Powder Diffraction data, Laboratory of Crystallography, University of Geneva, Switzerland, 2000.
[23] R. Shirley, CRYSFIRE: A Powder Indexing Suite, Software of the Collaborative Computational Project Number 14 (CCP14), School of Human Sciences, University of Surrey, UK, 1999.
[24] J. Laugier, B. Bochu, CHECKCELL: A Software Performing Automatic Cell/Space Group Determination, Collaborative Computational Project Number 14 (CCP14), Laboratoire des Materiaux et du Genie Physique de l'Ecole Supérieure de Physique de Grenoble, France, 2000.
[25] J. Rodríguez-Carvajal, FULLPROF: A Program for Rietveld Refinement and Pattern Matching Analysis. In Abstract of the Satellite Meeting on Powder Diffraction of the XV Congress of the International Union of Crystallography, Toulouse, France, 1990.
[26] L.M. González-Méndez, F.L. Cumbrera, M.C. García-Cuesta, F. Sánchez-Bajo, A.L. Ortiz, F.J. Higes-Rolando, F. Luna-Giles, Mater. Lett. 58 (2004) 672.
[27] M.C. García-Cuesta, A.M. Lozano, J.J. Meléndez-Martínez, F. Luna-Giles, A.L. Ortiz, L.M. González-Méndez, F.L. Cumbrera, J. Appl. Crystallogr. 37 (2004) 993.
[28] F.J. Barros-García, A. Bernalte-García, F.L. Cumbrera, A.M. Lozano-Vila, F. Luna-Giles, J.J. Meléndez-Martínez, A.L. Ortiz, Polyhedron 24 (2005) 1975.
[29] C. Cohen-Addad, Acta Crystallogr., Sect. B 38 (1982) 1753.
[30] F.H. Allen, Acta Crystallogr., Sect. B 58 (2002) 380.
[31] I.J. Bruno, J.C. Cole, P.R. Edington, M. Kessler, C.F. Macrae, P. McCabe, J. Pearson, R. Taylor, Acta Crystallogr., Sect. B 58 (2002) 389.
[32] F.J. Barros-García, A. Bernalte-García, F.J. Higes-Rolando, A.M. Lozano-Vila, F. Luna-Giles, E. Viñuelas-Zahínos, Polyhedron 24 (2005) 129.
[33] M. Joseph, V. Suni, M.R. Prathapachandra Kurup, M. Nethaji, A. Kishore, S.G. Bhat, Polyhedron 23 (2004) 3069.

[34] A.B.P. Lever, Inorganic Electronic Spectroscopy, second ed., Elsevier, Amsterdam, 1984.
[35] G.A. van Albada, W.J.J. Smeets, A.L. Spek, J. Reedijk, Inorg. Chem. Acta 299 (2000) 35.
[36] N. Ray, S. Tyagi, B. Hathaway, J. Chem. Soc., Dalton Trans. (1982) 143.
[37] J. Foley, S. Tyagi, B.J. Hathaway, J. Chem. Soc., Dalton Trans. (1984) 1.
[38] R.J. Dudley, B.J. Hathaway, P.G. Hodgson, J. Chem. Soc., Dalton Trans. (1972) 882.
[39] O.R. Rodig, T. Brueckner, B.K. Hurlburt, R.K. Schlatzer, T.L. Venable, J. Chem. Soc., Dalton Trans. (1981) 196.
[40] C.E. Baxter, O.R. Rodig, R.K. Schlatzer, E. Sinn, Inorg. Chem. 18 (1979) 1918.
[41] E.M. Gouge, J.F. Geldard, Inorg. Chem. 17 (1978) 270.
[42] G. Albertin, E. Bordignon, A.A. Orio, Inorg. Chem. 14 (1975) 1411.
[43] B.J. Hathaway, J. Chem. Soc., Dalton Trans. (1972) 1196.
[44] I.M. Procter, B.J. Hathaway, P.G. Hodgson, J. Inorg. Nucl. Chem. 34 (1972) 3689.
[45] B.J. Hathaway, in: G. Wilkinson, R.D. Gillard, J.A. McCleverty (Eds.), Comprehensive Coordination Chemistry, The Synthesis, Reactions, Properties and Applications of Coordination Compounds, vol. 5, Pergamon, Oxford, 1987, p. 533.
[46] B.J. Hathaway, D.E. Billing, Coord. Chem. Rev. 5 (1970) 143.
[47] M. Shakir, S.P. Varkey, F. Firdaus, P.S. Hameed, Polyhedron 13 (1994) 2319.
[48] B. Singh, R.N. Singh, R.C. Aggarwal, Polyhedron 4 (1985) 401.
[49] M.M. Mostafa, M.A. Khattab, K.M. Ibrahim, Polyhedron 2 (1983) 583.
[50] J. Nelson, S. Martin Nelson, W.D. Perry, J. Chem. Soc., Dalton Trans. (1976) 1282.
[51] J. Pons, A. Chadghan, J. Casabó, A. Álvarez-Larena, J.F. Piniella, J. Ros, Polyhedron 20 (2001) 2531.
[52] E. Viñuelas-Zahínos, M.A. Maldonado-Rogado, F. Luna-Giles, F.J. Barros-García, Polyhedron 27 (2008) 879.
[53] F.J. Barros-García, A. Bernalte-García, F.J. Higes-Rolando, F. Luna-Giles, M.A. Maldonado-Rogado, E. Viñuelas-Zahínos, Inorg. Chim. Acta 357 (2004) 1457.
[54] F.J. Barros-García, A. Bernalte-García, F.J. Higes-Rolando, F. Luna-Giles, A.M. Pizarro-Galán, E. Viñuelas-Zahínos, Z. Anorg. All. Chem. 631 (2005) 1898.
[55] F.J. Barros-García, A.F. Luna-Giles, M.A. Maldonado-Rogado, E. Viñuelas-Zahínos, Polyhedron 24 (2005) 2972.
[56] A. Bernalte-García, A.M. Lozano-Vila, F. Luna-Giles, R. Pedrero-Marín, Polyhedron 25 (2006) 1399.
[57] M.A. Maldonado-Rogado, E. Viñuelas-Zahínos, F. Luna-Giles, A. Bernalte-García, Polyhedron 26 (2007) 1173.